Optical Engineering

OpticalEngineering.SPIEDigitalLibrary.org

# How to assess good candidate molecules for self-activated optical power limiting

Hampus Lundén
Eirik Glimsdal
Mikael Lindgren
Cesar Lopes

SPIE.

Hampus Lundén, Eirik Glimsdal, Mikael Lindgren, Cesar Lopes, "How to assess good candidate molecules for self-activated optical power limiting," *Opt. Eng.* **57**(3), 030802 (2018), doi: 10.1117/1.OE.57.3.030802.

TUTORIAL

# How to assess good candidate molecules for self-activated optical power limiting

**Hampus Lundén,[a,b,*] Eirik Glimsdal,[c,d] Mikael Lindgren,[b,d] and Cesar Lopes[a]**
[a]FOI, Swedish Defence Research Agency, Linköping, Sweden
[b]Linköping University, Department of Physics, Chemistry and Biology (IFM), Linköping, Sweden
[c]Norwegian Defence Research Establishment (FFI), Kjeller, Norway
[d]Norwegian University of Science and Technology (NTNU), Department of Physics, Trondheim, Norway

**Abstract.** Reverse saturable absorbers have shown great potential to attenuate laser radiation. Good candidate molecules and various particles have successfully been incorporated into different glass matrices, enabling the creation of self-activated filters against damaging laser radiation. Although the performance of such filters has been impressive, work is still ongoing to improve the performance in a wider range of wavelengths and pulse widths. The purpose of this tutorial is, from an optical engineering perspective, to give an understanding of the strengths and weaknesses of this class of smart materials, how relevant photophysical parameters are measured and influence system performance and comment on the pitfalls in experimental evaluation of materials. A numerical population model in combination with simple physical formulas is used to demonstrate system behavior from a performance standpoint. Geometrical reasoning shows the advantage of reverse saturable absorption over nonlinear scattering due to a fraction of scattered light being recollected by imaging system optics. The numerical population model illustrates the importance of the optical power limiting performance during the leading edge of a nanosecond pulse, which is most strongly influenced by changes in the two-photon absorption cross section and the triplet linear absorption cross section for a modeled Pt-acetylide. This tutorial not only targets optical engineers evaluating reverse saturable absorbing materials but also aims to assist researchers with a chemistry background working on optical power limiting materials. We also present photophysical data for a series of coumarins that can be useful for the determination of quantum yields and two-photon cross sections and show examples of characterization of molecules with excited triplet states.  [DOI: 10.1117/1.OE.57.3.030802]

Keywords: optical power limiting; reverse saturable absorption; photophysical parameters; measurement.

Paper 171935T received Dec. 4, 2017; accepted for publication Jan. 31, 2018; published online Mar. 6, 2018.

## 1 Introduction

Lasers can damage optical sensors such as the eye due to optical focusing of electromagnetic radiation.[1,2] To protect sensors from damage over a broad band of threat laser wavelengths against both single or multiple pulses, without degrading the image by color filters, self-activated optical power limiters are used.[3–5] These protection devices are needed in, for example, military applications, where color filters only would give partial protection and/or degrade situational awareness.[3,5]

For useful protection against dangerous laser radiation, multiple demands are placed on a protection device.[5] The fundamental objective is to limit the transmitted intensity or pulse energy while degrading optical sensor performance as little as possible.[5] A central parameter is the dynamic range of the protective system

$$OD_{\mathrm{sys}} = -\log_{10}\frac{E_T}{E_{\mathrm{Dam}}}, \tag{1}$$

where $E_T$ is the pulse energy transmitted to the sensor, and $E_{\mathrm{Dam}}$ is the failure threshold of the protective device.[5] A desirable dynamic range for eye protection is an optical density of $OD_{\mathrm{sys}} = 4$ while having a linear transmission of at least 40%.[5] Note should be taken that $E_{\mathrm{Dam}}$ sometimes is defined relative to sensor damage level, leading to a demand of $OD_{\mathrm{sys}} \geq 0$ for the protective device.[6] Sources of system performance degradation include color distortion, low linear transmission, weight, physical size, and numerical aperture constraints.[5] For imaging systems, the importance of protective device optical quality should not be underestimated.

The performance of an optical power limiting (OPL) material or protective device is always implicitly or explicitly defined relative to the properties of the laser radiation it is intended to protect against. Two central parameters are wavelength and temporal pulse width.[5] For many self-activated protection mechanisms, the laser radiation needs to be focused to attain the nonlinear response. The transverse beam profile in the focus, as well as the temporal pulse shape, has an impact on OPL performance.[7,8]

Several different physical mechanisms have been proposed and utilized to attenuate damaging laser radiation.[2,5,6,9] A functional classification scheme often employed is to categorize the means of OPL as nonlinear refraction, nonlinear absorption, and/or nonlinear scattering. For practical optical design reasons discussed in Sec. 2, nonlinear absorption as the dominant mechanism is preferable to avoid a fraction of the radiation refracted/scattered being recollected by the optics.

*Address all correspondence to: Hampus Lundén, E-mail: hampus.lunden@foi.se

Reverse saturable absorption (RSA) occurs when the excited state absorption is larger than the ground state absorption of a material.[10] From the OPL perspective, RSA is an often employed mechanism to attenuate laser radiation.[6] In a simplified manner, the behavior of a RSA material can be described by

$$\frac{dI}{dz} = -[N\sigma_G + N_{ES}(\sigma_{ES} - \sigma_G)]I, \tag{2}$$

where $I$ is the intensity, $N$ is the numerical density of RSA molecules, $N_{ES}$ is the numerical density of RSA molecules in the excited state, $\sigma_G$ is the absorption cross section in the ground state, and $\sigma_{ES}$ is the absorption cross section in the excited state.[9] When $\sigma_{ES} \gg \sigma_G$ and the excitation into the excited state is sufficiently efficient and quick, a so-called "cut-off level" is achieved, where the transmitted intensity is comparatively constant relative to incoming intensity.[6,9] An illustrative classification scheme is the distinction between instantaneous and accumulative nonlinearities, the former depending on intensity while the latter on fluence.[9] Linear absorption into the excited state is an accumulative process as long as its lifetime is long compared with the laser pulse.[9]

The RSA of molecules has often been explained by a five-level population model.[9,11–16] It consists of three singlet states and two triplet states connected with an intersystem-crossing time, $\tau_{ISC}$, see Fig. 1. Wavelength-dependent linear absorption cross sections, two-photon absorption cross sections, and decay times are used to connect the states, see Sec. 4 for an overview.

Two-photon absorption (TPA) is an instantaneous mechanism, where two photons are absorbed together.[9] Although its intensity dependence makes it a mechanism suitable for shorter subnanosecond pulse lengths, in combination with RSA it can also increase the performance for nanosecond OPL.[17–19] This combination of mechanisms is sometimes called three-photon absorption (3PA).[17]

Early promising materials for OPL include King's complex and C-60 with variants.[9,20,21] Both King's complex and C-60 variants show both RSA and nonlinear scattering in solution.[9,20,21] Although these and other classes of chromophores, such as porphyrins,[15,16] show promising nonlinearities, performance is hampered by linear absorption in the visible wavelength region.[22–24] Pt-acetylides show good OPL response throughout the visible wavelength band while retaining low linear absorption.[11,22,23,25–29]

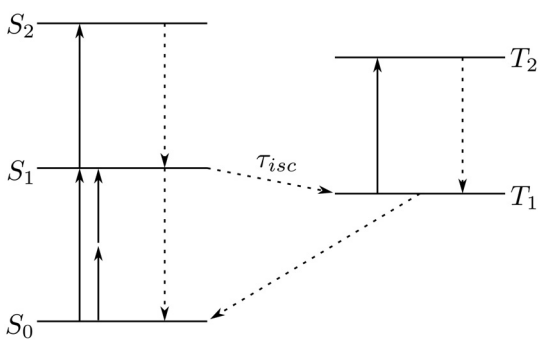


**Fig. 1** Jablonski diagram of a five-level population model for RSA molecules.[9,11–16]

For practical applications, bulk solid materials have obvious advantages over liquids.[24,30] Pt-acetylides have been doped into PMMA (polymethyl methacrylate) matrices, producing OPL filters of good optical quality.[24,31,32] By a more recent sol–gel method, MTEOS (methyltriethoxysilane) glasses have been created with extremely high concentrations of Pt-acetylides of up to 400 mM.[30] The solubility of chromophores and the dispersion ability of nanoparticles are vital properties in the preparation of doped glasses.[24,30,33–37] For MTEOS glasses, it is possible to control cavity size, i.e., tuning the exposure of the chromophores to oxygen quenching.[30]

Recent work in the OPL research field includes efforts to increase the span of pulse lengths and the range of wavelength response. By using a dense estradiol matrix protecting a donor–acceptor system against quenching, Hirata et al.[38] were able to demonstrate OPL for weak incoherent light. A multitude of different methods to protect the triplet state of chromophores against quenching have been investigated.[39] The design of chromophores with effective RSA in new wavelength ranges or having a more advantageous nonlinear performance to linear absorption trade-off is ongoing.[17,40,41]

To gain an understanding of the behavior of RSA materials, the five-level model above is often implemented as a numerical population model.[12,13,18,19,28,35,42] These are often coupled to beam-propagation models to simulate the effect of a material with depth and the shape of the laser spot.[13,18,43,44] In Sec. 4, the implementation details of a simplified model are given. It was previously used to explain the impact on RSA from improved two-photon absorption (2PA) by field enhancement.[34,35] These models require several material parameters, such as decay times and absorption cross sections, to have predictive value. The impact on performance by changing these parameters is demonstrated in Sec. 4.1.

In Sec. 3, an overview is given on the most often used measurement techniques for finding these parameters. Common pitfalls will also be described, including for common methods to demonstrate sample optical quality.

The purpose of this tutorial is to give the reader a qualitative understanding of what the impact of different material parameters are on OPL performance of RSA materials. First, this is made possible by time-resolved comparison plots of nonlinear absorption, previously developed to explain OPL enhancement for a Pt-acetylide chromophore by gold nanoparticles.[34] Second, an overview of relevant measurement techniques for optical material characterization, and their common pitfalls, is given.

## 2 Practical Use of RSA Materials for OPL–Implications for Evaluation

To increase the intensity of radiation on the self-activated filter, the laser beam is focused into the material.[3,9] Due to practical constraints on optical system compactness, a high $f$-number of the focusing optic cannot be expected.[3,5] A $f/5$ setup is often chosen when evaluating OPL materials[3,18,28,29,45–47] since it has a system configuration similar to many optical imaging systems.[3,5]

Although the influence of the focusing lens on spot size and intensity is obvious, the importance of the following radiation collecting lens should not be underestimated. Assuming the self-activated filter is placed inside the

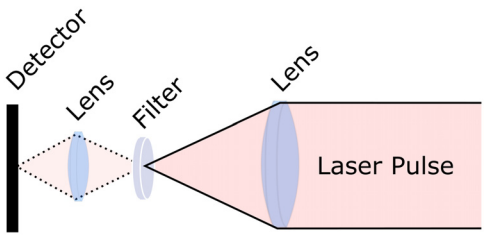


**Fig. 2** A self-activated filter placed inside the intermediary focus of a Keplerian telescope.

intermediary focus of a Keplerian telescope (see Fig. 2), the amount of scattered radiation collected by the optical system following the filter can be described by

$$I_{\text{out}} = \sigma\eta \frac{D^2}{16f^2} I_{\text{in}} = \sigma\eta \frac{1}{16(f/\#)^2} I_{\text{in}}, \tag{3}$$

where $I_{\text{out}}$ is the output intensity or fluence from the protective device, $\sigma$ is the fraction of radiation scattered, $\eta$ a factor (that can be more than 1) representing deviation from scattering with a perfectly spherical distribution, $D$ is the collecting lens' diameter, $f$ is the focal length, $I_{\text{in}}$ is the input intensity or fluence, and $f/\#$ is the $f$-number of the system. This equation can be derived by dividing the lens cross section with the area of a sphere of radius $f$. For an f/5 system with perfect spherical scattering, the collection efficiency would be $1/400$. This means that a compact protective device fulfilling application $f$-number constraints[3,5] and a required dynamic range[5] of $OD_{\text{sys}} > 4$ would be challenging to realize a self-activated filter with nonlinear scattering as its dominant mechanism. A similar argument could be made for OPL materials based on nonlinear refraction. The difficulty of blocking nonlinearly scattered and refracted light is known.[5] For RSA molecules, high phosphorescence efficiency is often seen as a desirable property as it indicates a high triplet yield. Since both fluorescence and phosphorescence would be recollected as scattered light, a high luminescence efficiency in a RSA material would be counter-productive for certain applications.

For laser protection applications, it can be expected that the entrance aperture of the system to be flooded by the laser, resulting in an approximately top-hat beam.[3] This causes an airy disk-like pattern in the focus, with large areas of low intensity.[48] A result of this is that a nonnegligible percentage of radiation is not nonlinearly attenuated by a self-activated filter.[48] Though, this light is not expected to be as damaging, because it is no longer being focused on the sensor area.[48] Apodization, being used in astronomical telescopes, is a well-known technique to remove the Airy rings.[49]

Although the low $f$-numbers of expected real-world systems result in a short Rayleigh range, thin films are susceptible to surface damage.[2] Second, the focal point of the optical system can move due to optical aberrations, necessitating thick filters.[3] It is difficult to keep particles in suspensions from agglomerating or to precipitate;[3] also, molecules in solution have had breakdown products fouling cuvette surfaces at high fluences.[50] For practical laser protection devices, these problems are best solved using solid-state materials. The requirement on thick bulk samples increases the impact of linear absorption. Induced color blindness/color distortion is unwanted for many applications.[4,5,51,52]

## 3 Measurements–Evaluation of OPL Materials

In laser protection research, there are two main techniques for evaluating the nonlinear performance of OPL materials: the intensity scanning usually made with an $f/5$ setup and the z-scan.[47,53] A more complete list of available measurement techniques can be found in Dini et al.'s[6] recent review. An overview of these two methods is found in Secs. 3.1 and 3.2. Their descriptions in this tutorial will focus on their strengths, weaknesses, and potential pitfalls.

In demonstration of glass sample quality, the standard method in the research field is photographing the samples lying on a piece of paper, often with the organization's logo on the paper. Although this method will show any cracks and bubbles, it is unsatisfactory since it is poorly suited to catch any refractive index variations in the glass. There are standards for specifying material imperfections,[54] but it would be overly complicated to use them for laboratory work. By instead photographing the samples at 70-cm (arm's length) distance with a far-away but detailed background, unwanted refractive index variations become visible.

### 3.1 *Intensity Scanning*

The most straightforward method to measure OPL performance is to vary the intensity of incoming radiation on the sample while measuring the transmitted output radiation. But considering the impact of optical geometry on OPL performance (Sec. 2), comparing results from different measurement setups is difficult. A $f/5$ setup, first published by Vincent et al., has been widely used in the research field.[3,18,28,29,45–47] Its strength lies in its similarity to expected real-world systems (Sec. 2).

In principle, a near top-hat shape collimated 2-cm diameter beam of known pulse energy enters a 2.5× magnification telescope. At 10 cm a focus is formed, where the sample is placed after the spot size has been characterized, often by a combination of knife-edge and camera measurements. The beam is recollimated by a 4-cm focal length lens and passed through an 8-mm aperture. The beam is then focused into a small aperture before striking the signal detector. The small aperture differs in size between different experimental setups and is used for removing scattered light at high fluences.[29] If measurements are done on high-quality glass samples, the aperture can be removed.[33] In setting up an OPL measurement setup, it is important to use achromatic lenses to cancel spherical aberrations, keeping the spot-size small.

When analyzing measurements on solid samples, the influence on OPL performance from damage mechanisms needs to be considered. The intensity scanning measurements require higher fluences than in the $Z$-scans. It is therefore standard procedure to translate the sample between each pulse or, in the case of solutions, to keep the pulse repetition rate low.[30,55] A relaxed definition of damage fluence level is the onset of when the transmittance falls abruptly from a single pulse. A stringent definition of damage is that no decrease of transmission is detected during several pulses on the same spot while also finding no damage in microscopy images.[37] This method is preferable for separating RSA from damage mechanisms. Other methods include photophysical measurements indicating RSA and ensuring that the nonlinear scattering from glass damage is low.

The acquired data are often presented as a point plot with each pulse represented by one point. The $x$-axis shows input

fluence [J/cm$^2$], whereas the $y$-axis shows either output energy [$\mu$J] or output fluence [J/cm$^2$]. The advantage of showing output energy is that damage levels of sensors such as the eye often is defined as such. Another popular way to present the data is an $x$-logarithmic input fluence versus transmittance plot.

When interpreting the data, it is important to consider the inherent weaknesses of the measurement technique. Even ideally, a clean cut-off level will not be achieved by a realistic RSA material due to the Airy fringes. More so, the setup is sensitive to laser beam quality and alignment errors. Therefore, performance comparisons between materials of similar performance should only be done during the same measurement campaign or with the help of reference samples.

For bulk glass materials, the positioning, depth wise, of the beam waist in the sample influences OPL performance due to linear absorption before the focus.[56] It is advisable to place the focus in the middle of the sample to avoid influence on OPL performance from surface damage.

A central drawback of the intensity scanning method mentioned by Dini et al.,[6] is that it is poorly suited to differentiate nonlinear refraction from nonlinear absorption. A labor-intensive method to alleviate this drawback is to remove the optics following the sample and replace them with an integrating sphere surrounding the sample.[33] This will recapture most of the nonlinearly scattered and/or refracted radiation, thereby nullifying the impact of these mechanisms.

### 3.2 *Z-Scan*

The $Z$-scan by Sheik-Bahae et al.[53] is a method where the sample is translated along a relatively low fluence laser beam through the focus. For a schematic overview, see Fig. 3. It is a method often used for its ability to deliver quantitative data on nonlinear optical parameters of the sample. The $Z$-scan is a model-based method, where the measured data are curve-fitted to a model with the nonlinear refraction and absorption coefficients

$$n(I) = n_0 + \gamma I, \tag{4}$$

$$\alpha(I) = \alpha_0 + \beta I. \tag{5}$$

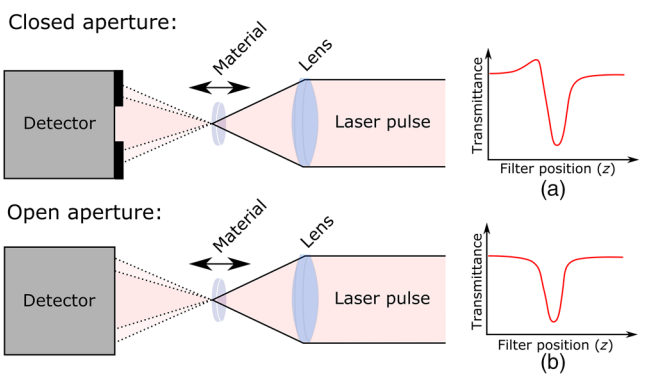


**Fig. 3** A schematic view of a $Z$-scan setup.[53] The upper right insert (a) shows the closed aperture transmittance when the material sample is transposed through the focus. It is the result of a combination of nonlinear refraction causing a widening or narrowing of the beam and nonlinear absorption. The lower right insert (b) shows the open aperture transmittance. Due to the absence of the limiting aperture, the impact of nonlinear refraction is small.

The two nonlinear parameters are differentiated by doing two different measurements, one with an open and one with a closed aperture in front of the sensor.[53] With a closed (small) aperture, there will be a larger impact on transmittance from a nonlinearly refracted beam as it becomes more focused or divergent.[53] Several improvements in the $z$-scan method have been introduced including thick samples, non-Gaussian laser beams, and higher sensitivity.[7,57–59] The $Z$-scan technique is capable of measuring 2PA and nonlinear refraction at large wavelength ranges from the UV to the IR.[60,61]

High-quality $z$-scan measurements require a well-characterized beam, both spatially and temporally.[7] Sample optical quality needs to be considered, especially when measuring nonlinear refraction.[7] Nonlinear reflectance from sample surface can induce error in the measurements on solid materials with high absorption, but modern extensions of the $z$-scan method can handle this situation.[62]

When doing $z$-scan measurements, it is important to consider the applicability of the underlying model that is fitted. The timescale of the nonlinearity investigated compared with the laser pulse is of vital importance.[7] For RSA the ESA mechanism can be simplified to an equivalent $\beta$ parameter, but the results will not be comparable with other setups or laser pulse widths.[18] When measuring the 2PA of an RSA molecule as $\beta$, it is important to select a short enough laser pulse width compared with the population dynamics of the investigated molecule.[12] Numerical population models can be used to check this.[12]

The $Z$-scan method does not take nonlinear scattering into account.[63] To investigate materials with significant nonlinear scattering, the $Z$-scan has been augmented by placing a secondary detector off-axis.[37,64] Consider also, in measurements of nonlinearly scattered radiation, that the scattering might not be spherically homogenous.[65] For certain materials, an integrating sphere intensity scanning measurement is preferable.[33] Though, an off-axis detector should be considered in any $Z$-scan setup for detecting the presence of unexpected nonlinear scattering.

### 3.3 *Photophysical Measurements*

To gain an understanding of the behavior of RSA molecules, a first step is to make a detailed photophysical characterization of their basic properties. Several different measurements are usually performed depending on the nature of the optical process to be used for OPL. A brief step-by-step procedure is given here, with focus on organic dye molecules. Primarily, it is advantageous to first study the dyes in solution, where concentration can readily be controlled, and effects of different solvent interactions can be examined. These properties are very useful at a later stage if one seeks to integrate the molecular system into a solid matrix such as a sol–gel glass, polymer films, or other advanced nanomaterial systems. The optical absorption spectra along with the luminescence emission give the wavelength range and strength of the ground state absorption, along with the energy of the lowest excited state. Fast luminescence from (usually) singlet states decays typically between 1 and 100 ns and is called fluorescence. If there is efficient intersystem crossing, triplet states (or higher spin multiplets) can also be formed, and these decay as phosphorescence with a much slower rate, typically in the range 1 to 500 $\mu$s in solutions at room temperature. Thus, it is advantageous to also record the decay time of

the luminescence to distinguish rapidly decaying singlet states from phosphorescence and properly design the material for the OPL application.

### 3.3.1 *General appearance of linear absorption and emission processes*

Representative absorption and luminescence spectra of Coumarin 110 (C110) and Pt-octaethyl-porphyrin (Pt-OEP),[66] which both can be used as reference materials, are shown in Fig. 4. Pt-OEP has long-lived triplet states in solutions, such as THF and toluene. It gives bright phosphorescence if the solvent is evacuated from oxygen, like similar linear Pt-acetylide variants.[67,68] C110 can be used for the determination of quantum efficiency and TPA cross section (see below). In general, nonpolar organic solvents have higher solubility of oxygen and more care must be taken to evacuate it by, e.g., Argon-bubbling, as oxygen is a well-known quencher of triplet states. (Triplet states will be discussed later in this section.)

The associated lifetimes can be measured using time-resolved spectroscopy. By the use of time-correlated single photon counting (TC-SPC), lifetimes in the range ~50 ps to 1 $\mu$s can be determined (i.e., fluorescence).[69] Longer lifetimes due to phosphorescence can usually be measured directly with a fast photodiode or other schemes utilizing the photon counting PMT detector, such as multichannel scaling (MSC).[70] If an fs-laser is used for excitation, one can readily measure the two-photon absorption with the same data collection system (see below). An example of a system configuration is shown in Fig. 5.

Here, a tuneable Ti:Sapphire fs-laser with up-conversion unit is being used to study single photon excitation in the visible. The fundamental wavelength can then be used for studying multiphoton processes. By allowing pulsed lamps and LEDs, it is also possible to investigate phosphorescence with the same detection system. The pulse-picker is necessary to reduce the pulse repetition frequency (PRF) of the laser if longer lifetimes are to be investigated.[68,69] By scanning the monochromators, the spectral properties

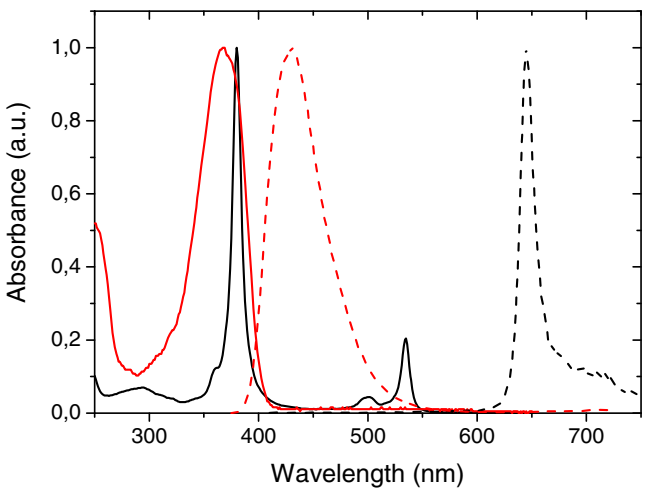


**Fig. 4** Absorption (solid) and luminescence (dashed) of Pt-OEP (black) and C110 (red). The solute molecules are dissolved in THF. The Pt-OEP sample was flushed with Argon gas for 8 min to remove oxygen that quench the phosphorescence.

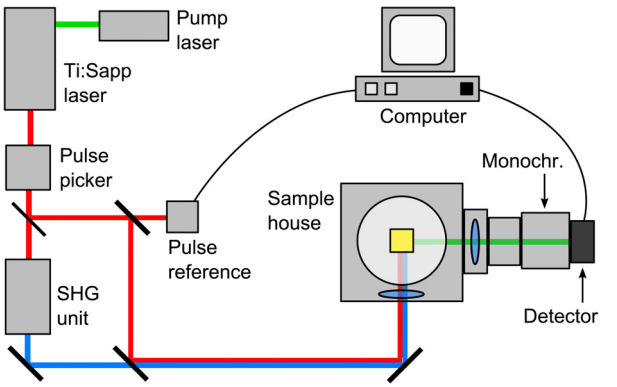


**Fig. 5** System layout for measurements of lifetimes and TPA cross section.

for a given excitation wavelength and pulse configuration can be systematically studied. A representative fluorescence lifetime decay of C110 and phosphorescence decay of Pt-OEP are shown in Fig. 6 (these correspond to the same samples as displayed in Fig. 4). It is emphasized that the Pt-OEP sample has been bubbled with argon gas to evacuate oxygen, which is a strong quencher of the triplet state.

### 3.3.2 *Quantum efficiency and two-photon absorption cross section for a series of reference dyes*

An important parameter is the quantum efficiency (QE) of the emission. This is the probability that an absorbed photon will give rise to emission. The maximum value is 1, and it means that all excitations at a certain wavelength result in luminescence. To determine the QE, it is advantageous to record and integrate the emission for several concentrations, where the optical absorbance is not too high. This ensures that the optical transition processes are "independent" and that the emitting molecular system is not quenched by or stimulated by photophysical reactions from surrounding fellow molecules. The quantum efficiency and two-photon cross section is here examined for a series of reference molecules as shown in Fig. 7.

The measurements are performed using a reference dye with known properties, such as fluorescein (QE and TPA cross section) and quinine sulfate (QS). Here, it is important that the solvent used for the reference should have the correct pH (basic for fluorescein and acidic for QS, see notes in Table 1). It is important that the "unknown sample" and the reference sample have some spectral overlap, so that the full emission band can be recorded at the same excitation wavelength.[69,71] For a series of concentrations, the associated integrated emission spectrum is plotted versus absorbance for each sample, at the relevant excitation wavelength. The resulting slope is proportional to the QE, and thus the unknown sample can be measured from the equation

$$\frac{\mathrm{QE}_X}{\mathrm{QE}_Y} = \frac{\mathrm{Slope}_X}{\mathrm{Slope}_Y} \cdot \frac{n_X^2}{n_Y^2}, \tag{6}$$

where $X$ represents the unknown sample, and $Y$ is the reference sample with known QE. If the solvents used are different one has to compensate with the refractive index $n^2$ in the expression.[72] The top panels of Fig. 8 show absorption and

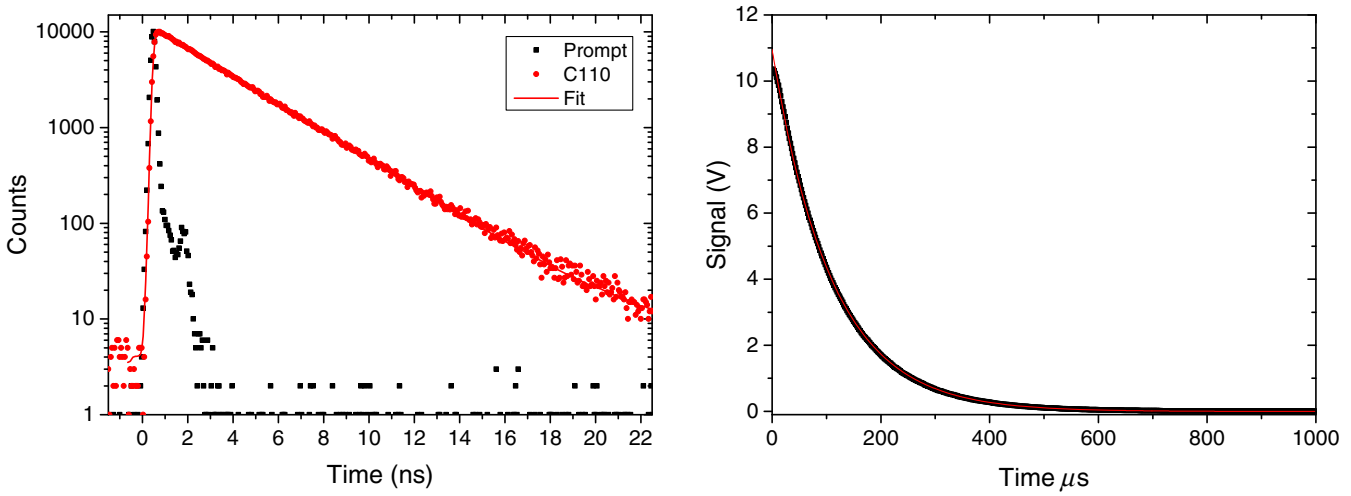


**Fig. 6** (a) The logarithm of the TC-SPC decay trace of C110 yielding a single decay constant of 2.9 ns. The excitation wavelength was 403 nm and the emission recorded at 440 nm. (b) The phosphorescence decay of Pt-OEP for excitation at 375 nm and emission at 645 nm. The decay time is 108 $\mu$s. The solid lines are monoexponential fits.

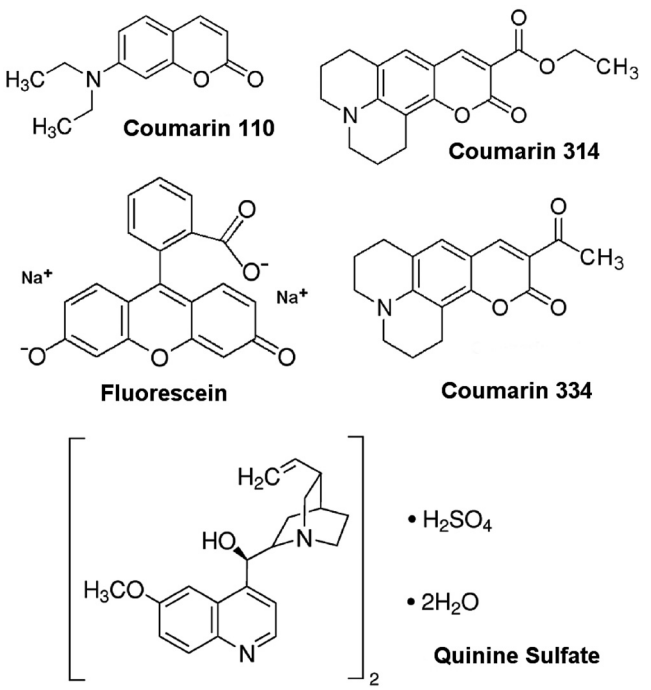


**Fig. 7** Chemical structures for molecules that were examined in terms of quantum efficiency and two-photon absorption cross section. All samples were purchased from Sigma–Aldrich and used as received.

emission spectra of a series of coumarins together with reference molecules fluorescein and quinine sulfate (QS).

The lower panels show data from samples of various concentrations, where the integrated emission spectrum is plotted versus the associated absorbance at the same excitation wavelength. As long as the concentration is low enough, corresponding to an absorption of OD ~0.10, the plots are linear and the slope is proportional to the QE. The photophysical data from a series of coumarins along with the reference compounds are summarized in Table 1.

Once the emission spectrum and QE are known, one can readily determine the two-photon absorption (TPA)

**Table 1** Photophysical parameters of examined coumarins and reference molecules in Fig. 7. 10-$\mu$M solutions were used to measure the extinction coefficient. "Low enough" concentrations (typically below 1 $\mu$M) were used to determine emission properties.

| Sample | $\lambda_{abs}$ (nm) | $\lambda_{em}$ (nm) | $\varepsilon$ ($10^4$ OD $M^{-1}$ $cm^{-1}$) | $\tau$ (ns) | QE |
|---|---|---|---|---|---|
| Fluorescein[a] | 490 | 514 | 8.8[71,73] | 4.2 | 0.92[71] |
| QS[b] | 347 | 442 | 5.5 | 19.5 | 0.55[71] |
| C110[c] | 370 | 423 | 2.4 | 2.9 | 0.62 |
| C334[c] | 444 | 476 | 3.6 | 3.0 | 0.83 |
| C314[c] | 427 | 458 | 3.5 | 2.8 | 0.93 |
| C314[d] | 437 | 474 | 4.5[74] | 3.3 | 0.85 |

[a]Solvent 0.1 M NaOH.
[b]Solvent 0.5 M $H_2SO_4$.
[c]Solvent THF.
[d]Solvent ethanol.

cross section from the emitted fluorescence spectrum.[75,76] This is an alternative method to the $z$-scan technique described in Sec. 3.2. Usually, $z$-scan needs quite high concentrations to give the TPA cross section, where fluorescence-based techniques are much more sensitive, and it is possible to go down to $\mu$M levels. Here, a laser with short pulse length must be utilized (up to 200 fs) as longer pulses can give spurious effects from sequential excited state absorption, e.g., from triplet states. Moreover, for the same reason, a low enough PRF must be used to ensure that possible triplet states formed by intersystem crossing have decayed to the singlet ground state (see discussion in Sec. 3.2). The determination of TPA cross- section for a range of PRFs is a simple way of checking if parasitic excited state absorption is present, see Glimsdal et al.[77] In this work, the relative amount of fluorescence collected by two-photon excitation of 50-$\mu$M samples was analyzed.

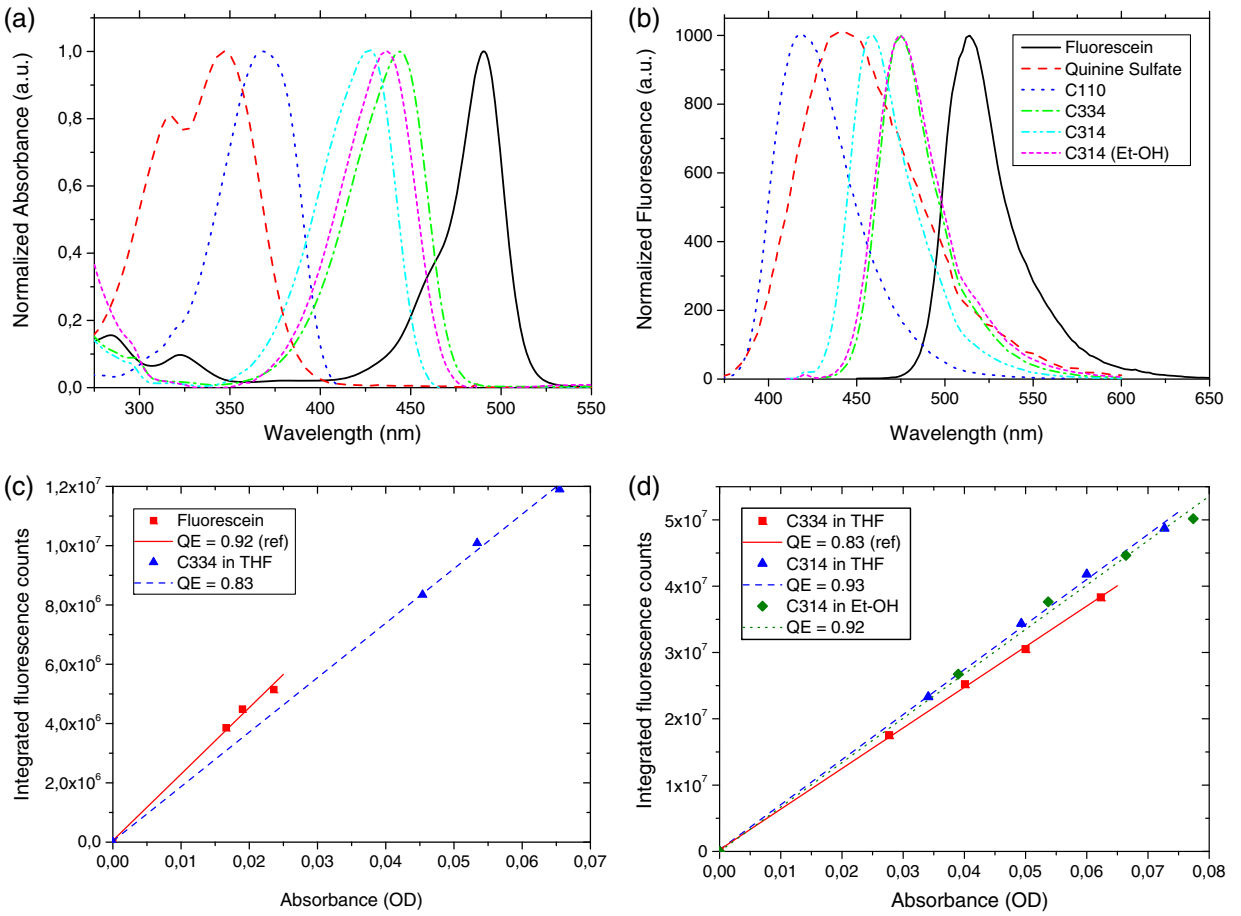


**Fig. 8** Absorption (a) and emission (b) spectra of a series of coumarins along with the reference materials fluorescein and quinine sulfate. The amplitude of the spectra is normalized to 1 to easily show spectral shifts and position. (c) and (d) Representative results of plots to obtain quantum efficiency from the slope of integrated fluorescence versus absorbance. For more details, see Table 1.

The TPA cross section can be found when the quantum efficiencies of a reference sample are known from the expression of Albota et al.[78]

$$\frac{\langle F(t)\rangle_{\mathrm{ref}}}{\langle F(t)\rangle_{\mathrm{new}}} = \frac{(\mathrm{QE}_{\mathrm{ref}})\eta_{\mathrm{ref}}\sigma^{(2)}_{\mathrm{ref}}C_{\mathrm{ref}}\langle P_{\mathrm{ref}}(t)\rangle^2 n_{\mathrm{ref}}}{(\mathrm{QE}_{\mathrm{new}})\eta_{\mathrm{new}}\sigma^{(2)}_{\mathrm{new}}C_{\mathrm{new}}\langle P_{\mathrm{new}}(t)\rangle^2 n_{\mathrm{new}}}, \tag{7}$$

where QE, $\eta$, and $\sigma^{(2)}$ are the quantum yield, measurement collection coefficient, and TPA cross section, respectively. $C$ is the sample concentration, $n$ is the refractive index, $\langle F(t)\rangle$ is the measured time-averaged, spectrally integrated fluorescence, and $\langle P(t)\rangle$ is the time-averaged excitation pulse profile. The indices "ref" and "new" refer to the reference sample (such as fluorescein) and the new, unknown sample, respectively. Using equivalent sample cells and concentrations while using the same excitation and measurement configuration (power, emission collection, etc.), the expression simplifies and the TPA cross section is readily determined against the reference sample. Here, fluerescein was used as a reference material for those coumarins with 2PA in a compatible wavelength range. The 2PA of the other coumarins were found by systematically varying the excitation wavelength

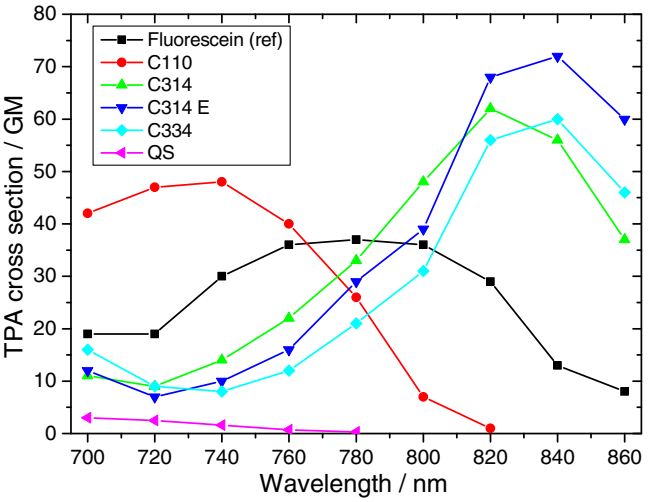


**Fig. 9** TPA cross section obtained from fluorescence yields for various excitation wavelengths in the range 700 to 860 nm. Fluorescein was used as reference material. All samples at 50-$\mu$M concentration. Solvents and other parameters are given in Table 1.

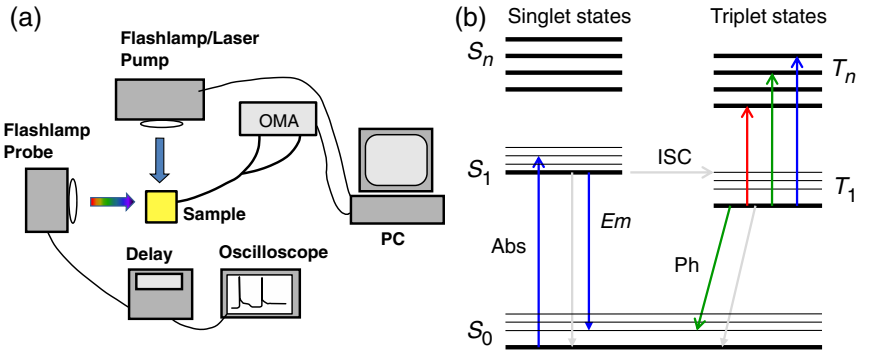


**Fig. 10** (a) Schematic of transient absorption measurement in the $\mu$s to ms range. (b) Scheme for populating excited triplet states. The gray line indicates intersystem crossing (ICS) from the singlet to the triplet state.

extrapolating step by step. Thus, useful TPA cross sections for serving as reference molecules were found to be in the range 5 to 75 GM, with fluorescence QE ranging from 0.62 to 0.93.

### 3.3.3 *Characterization of triplet states and phosphorescence*

As shown in Figs. 4 and 6, certain molecular systems with strong spin-orbit coupling such as Pt-OEP give rise to luminescence slowly decaying as phosphorescence. At room temperature and in solutions, such triplet states are usually very vulnerable to collisions and vibration of the solvent structure, making it a quite rare phenomenon. Therefore, one needs alternative methods to detect and characterize such triplet states. As discussed in other sections, the triplet state is very efficient as excited state for absorption processes that give rise to OPL. A schematic of a system for transient triplet–triplet absorption is shown in Fig. 10.

In this setup, a fast flashlamp (typically 1 to 5 $\mu$s), or a laser (typically in ns regime), is first used to pump/excite the molecular system via the singlet–singlet absorption (Figs. 4 and 8). If there is sufficient intersystem crossing to the triplet manifold, excited triplet states will accumulate [$T_1$ in Fig. 10(b)]. Synchronously with the pump another source (probe) is fired and used to record the absorption in the excited triplet state, usually with a lifetimes in the 0.1 $\mu$s to 100 $\mu$s range. In Fig. 11(a), such transient absorption spectra are recorded. The transient absorption spectrum is calculated using several reference measurements: the signal in the absence of probe pulse and the signal in the absence of pump pulse. For a detailed description of the data processing along with example molecules, see Glimsdal et al.[79] As can be seen in this example, the absorption spectrum is dramatically different from the ground state absorption shown with the dashed line. This is a sample that can be used for OPL measurements as the transparent range above 400 nm becomes considerably darkened by the excited triplet state upon excitation.

By varying the delay between the pump and the probe, one obtains information of the excited triplet state in question and the triplet state lifetime can be calculated [see Fig. 11(b)]. The advantage of the OPL measurement is that it gives directly some important parameters for calculating the performance: the spectral extension and extinction coefficient of the excited triplet state as well as its lifetime.

To investigate the faster dynamics of the system, such as intersystem-crossing time, ultrafast transient absorption

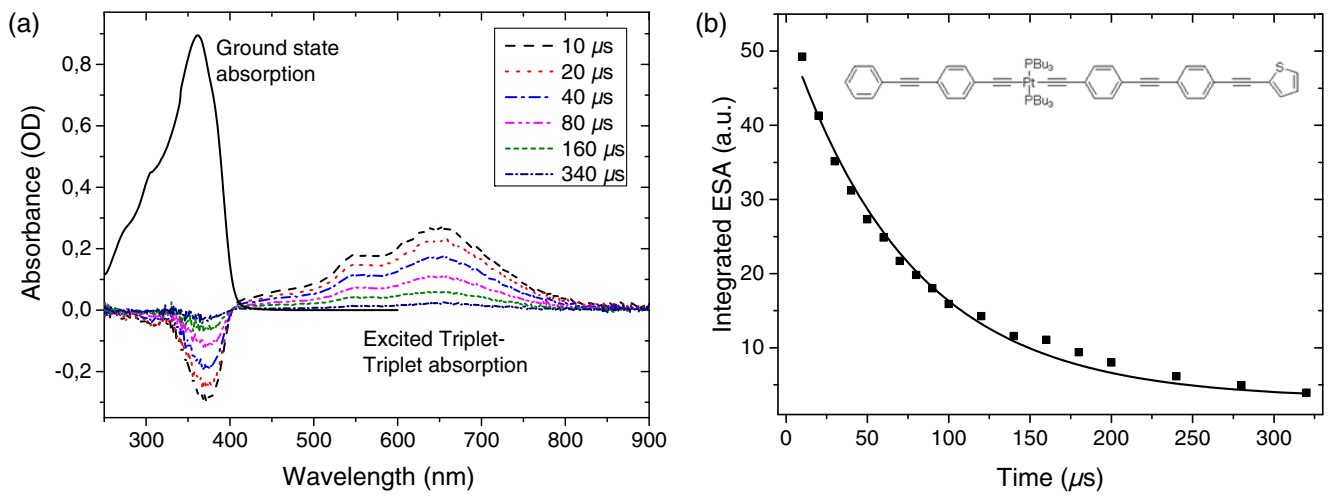


**Fig. 11** (a) Time-resolved triplet transient absorption spectra (solid lines) recorded at different delay times along with the ground state absorption spectrum (dashed line). (b) Decay trace giving information about the triplet state kinetics formed by integrating the absorption between 500 to 800 nm for varying delay times. The solid line is a fit with decay constant 76 $\mu$s. The molecular structure of the sample is depicted (THF was used as solvent).

measurements can be used.[80–82] These measurements split the femtosecond to picosecond pulses into a pump and probe beam. The probe beam is delayed by a variable delay line. The temporally well-characterized pump pulse is used to excite the sample while white continuum pulses are generated from the probe beam. By varying the delay time, a time-resolved spectrum of the ESA can be measured. Fluorescence up-conversion can be used to further investigate the ultrafast kinetics of the excited singlet state.[80]

## 4 Numerical Population Models

Numerical population models are an often used tool in the laser protection research field.[12,13,18,19,28,35,42] Although the coupling of population models with beam-propagation models have been fruitful,[13,18,43,44] this tutorial will focus on single point models for brevity. With a single point model, it is still possible to check the validity of 2PA $z$-scan measurements regarding premature population of the excited state.[12] This tutorial will use a numerical population model to explain the impact of changing different parameters in a simplified five-level model on OPL performance.

From a general perspective, the stepwise numerical population model can be described by

$$dN_i^+ = \sum_j \sigma_{ji} J \Delta t N_j + \sum_j \omega_{ji} J^2 \Delta t N_j + \sum_j \frac{\Delta t}{\tau_{ji}} N_j, \tag{8}$$

$$dN_i^- = \sum_j \sigma_{ij} J \Delta t N_i + \sum_j \omega_{ij} J^2 \Delta t N_i + \sum_j \frac{\Delta t}{\tau_{ij}} N_i, \tag{9}$$

$$dN_i = dN_i^+ - dN_i^-, \tag{10}$$

where $dN_i$ is the change in population density of the $i$'th state, $\sigma_{ij}$ is the linear absorption cross section from the $i$'th to the $j$'th state, $J$ is the photon flux, $\Delta t$ is the simulation time-step length, $N_i$ is the population density of the $i$'th state, $\omega_{ij}$ is the 2PA cross section from the $i$'th to the $j$'th state, and $\tau_{ij}$ is the decay time from the $i$'th to the the $j$'th state. These step update equations are implemented by a generic matrix formalism. Either manually or automatically $\Delta t$ must be kept short enough that the change in state population never exceeds the population of a single state. The attenuation coefficient can be described by

$$\alpha = \sum_{i,j} (\sigma_{ij} + \omega_{ij} J) \Delta t N_i. \tag{11}$$

Under the assumption that the intersystem crossing is fast enough that the higher $S_N$ states can be ignored and the relaxation from the $T_N$ state is instantaneous, the model can be described by the three-dimensional matrices

$$\sigma_{ij} = \begin{bmatrix} 0 & \sigma_S & \sigma_F \\ 0 & 0 & 0 \\ 0 & 0 & \sigma_T \end{bmatrix}, \tag{12}$$

$$\omega_{ij} = \begin{bmatrix} 0 & \omega_S & 0 \\ 0 & 0 & 0 \\ 0 & 0 & 0 \end{bmatrix}, \tag{13}$$

$$\tau_{ij} = \begin{bmatrix} \infty & \infty & \infty \\ \tau_S & \infty & \tau_{\mathrm{ISC}} \\ \tau_T & \infty & \infty \end{bmatrix}, \tag{14}$$

where $\sigma_S$ is the absorption cross section of the $S_0$ to $S_1$ transition, $\sigma_F$ is the absorption cross section of the forbidden $S_0$ to $T_1$ transition,[11] $\sigma_T$ is the $T_1$ to $T_N$ ESA cross section, $\omega_S$ is the 2PA cross section for $S_0$ to $S_1$, $\tau_{\mathrm{ISC}}$ is the intersystem-crossing time, and $\tau_T$ is the triplet lifetime. To include the effects of an intersystem crossing quantum efficiency, $\phi_{\mathrm{ISC}}$, a decay of the $S_1$ state is added[35]

$$\tau_S = \tau_{\mathrm{ISC}} \frac{\phi_{\mathrm{ISC}}}{1 - \phi_{\mathrm{ISC}}}. \tag{15}$$

The model parameters used in this tutorial are based on the well-investigated PE2 molecule, a Pt-acetylide RSA chromophore.[12,34,83] The model laser wavelength is 600 nm, fluence 10 J/cm$^2$, and temporally Gaussian with a pulse width of 5 ns.[34,35] The concentration is set to 50 mM. $\sigma_S$ is 0.2 M$^{-1}$ cm$^{-1}$.[83] $\sigma_F$ is set to 0 M$^{-1}$ cm$^{-1}$ since 600 nm is outside the expected wavelength range of this transition.[11] $\sigma_T$ is set to 42,000 M$^{-1}$ cm$^{-1}$.[83] $\omega_S$ is 290 GM.[12] $\phi_{\mathrm{ISC}}$ is 92%.[83] $\tau_{\mathrm{ISC}}$ is 300 ps.[12] $\tau_T$ is set to 42 $\mu$s.[83] These parameters need to be converted into units compatible to the photon flux $J$ in photons/cm$^2$/s.[84]

To visualize the impact in changing these variables, we define the time-resolved attenuation coefficient improvement function as

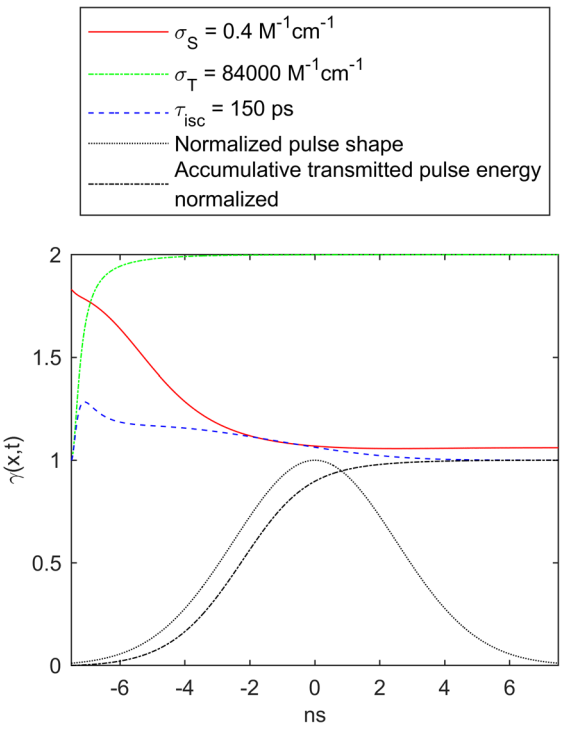


**Fig. 12** Time-resolved attenuation coefficient improvement function for PE2 from doubling linear absorption cross section, triplet absorption cross section, or halving the intersystem-crossing time. The normalized laser pulse shape is shown. Also, the accumulative transmitted pulse energy for the reference material is shown normalized to 1 in an effort to visualize part of the pulse where the OPL performance can be further improved.

$$\gamma(t) = \frac{\alpha(t)}{\alpha_{\mathrm{ref}}(t)}, \tag{16}$$

where $\alpha(t)$ and $\alpha_{\mathrm{ref}}(t)$ are the attenuation coefficients calculated for a material with perturbed and unchanged parameters, respectively.[34] Considering that the majority of radiation is transmitted at the start of the pulse,[48] the accumulative transmitted radiation normalized to one is plotted for the model with unchanged parameters. The focus depth is set to 30 $\mu$m.

### 4.1 *Model Results and Discussion*

The attenuation coefficient improvement function [Eq. (16)] was calculated for the model with one parameter changed in each case. The results are shown in Figs. 12 and 13.

Figure 12 shows how a doubling of $\sigma_S$ improves performance at the earliest stages of the pulse, but the improvement tapers off as the triplet state becomes populated. A doubled attenuation coefficient for the triplet state, $\sigma_T$, has a much larger impact for the part of the pulse where the most radiation is transmitted. Considering earlier numerical models of RSA molecules, this result was expected.[18,19] Twice as fast intersystem-crossing time, $\tau_{\mathrm{ISC}}$, do not show a large improvement in attenuation coefficient. This can be interpreted as that the intersystem-crossing time already is fast enough compared with the laser pulse width.

Figure 13 shows how twice as large 2PA improves the OPL performance at relevant parts of the pulse. This is expected since the dominant OPL mechanism of PE2 at 600 nm is 2PA.[85] The ability of 2PA to enhance RSA is well known.[17,19] Further improving the quantum yield of intersystem crossing from 92% did not improve OPL performance in any meaningful way. Changing the linear absorption to a direct forbidden transition into the triplet state did not improve the performance significantly during the most important parts of the pulse. This can be explained as a combination of a short enough $\tau_{\mathrm{ISC}}$ and high 2PA, $\omega_S$.

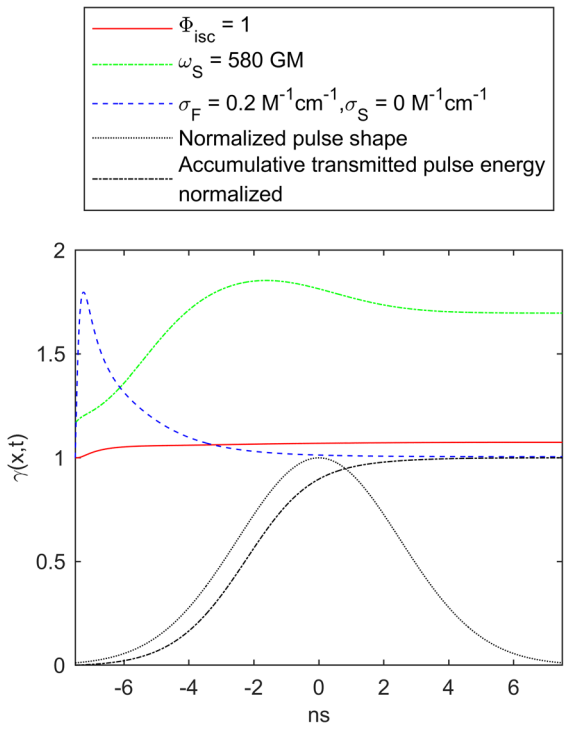


**Fig. 13** Time-resolved attenuation coefficient improvement function for PE2 from 100% quantum efficiency into the triplet state, double 2PA or a forbidden linear absorption directly into the triplet state. The normalized laser pulse shape is shown. Also, the accumulative transmitted pulse energy for the reference material is shown normalized to 1 in an effort to visualize part of the pulse where the OPL performance can be further improved.

### 4.2 *Impact of Temporal Pulse Shape*

The importance of laser temporal pulse shape on OPL behavior is known.[53,59] To give an estimate of the "error" resulting from a temporally multimode OPO laser, the normalized accumulative transmission is plotted for both a 5-ns FWHM Gaussian beam and a 5-ns perfect square signal. Both pulses are of 10 J/cm$^2$. The results in Fig. 14 indicate a problem to be aware of.

### 4.3 *Impact of Triplet Lifetime*

Due to the long triplet lifetime of PE2 compared with the simulated nanosecond pulse width, the triplet lifetime would have to be drastically shortened to influence OPL performance.

But for OPL of continuous wave (CW) laser radiation, a long triplet lifetime is central for performance.[38] The host-matrix influences triplet lifetime through quenching, for example, from oxygen or vibrations.[30,38] For a CW laser beam, the impact of 2PA is expected to be negligible compared with the pulsed case.

To visualize the impact of a long triplet lifetime on CW OPL, the model was slightly modified. At 600-nm laser wavelength the linear absorption cross section, $\sigma_T$, of PE2 is fairly low compared with 3.8 M$^{-1}$ cm$^{-1}$ at around 473 nm.[83] Though the ESA cross section, $\sigma_T$, at 473 nm is somewhat lower at 25,000 M$^{-1}$ cm$^{-1}$.[83] The modeled laser beam was set to 10 mW with an 18-$\mu$m beam waist diameter. The focus depth was kept at 30 $\mu$m. A highly doped sol–gel glass of 400 mM was simulated. The model assumes a matrix that is very efficient in shielding the PE2 triplet state, keeping the triplet lifetime at 42 $\mu$s.

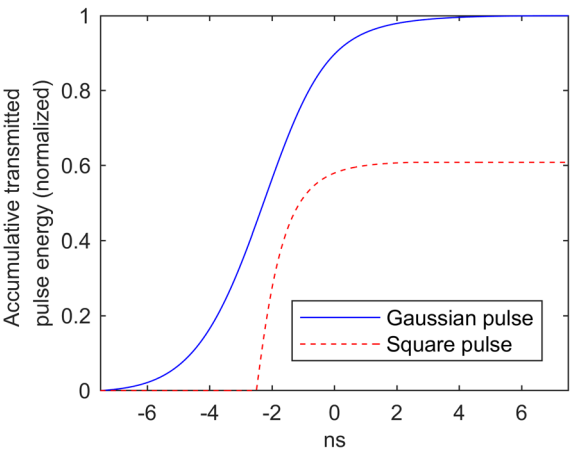


**Fig. 14** Comparison of accumulative transmitted pulse energy for a temporally Gaussian and square pulse. FWHM is 5 ns and the pulse energy 10 J/cm$^2$. The same PE2 model was used.

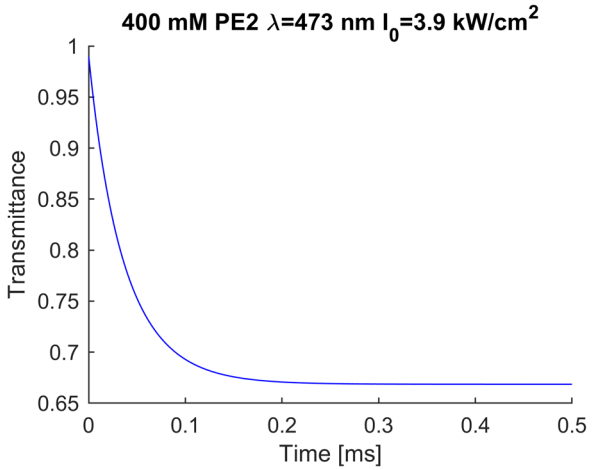


**Fig. 15** Simulated transmittance of a 400 mM PE2 doped sol–gel glass of a 10 mW 473 nm CW laser beam. Only the part of the glass that is in the focus is included in the simulation.

In Fig. 15, it is shown that a long triplet lifetime allows for a significant population in the triplet state, even for a relatively low intensity CW beam (compared with the pulsed case).

For measurements of CW OPL from RSA materials, Fig. 15 shows that it is important to do the measurements in a sufficiently time-resolved manner. The longer the triplet lifetime, the longer it will take for the triplet population to reach steady state. When simulating a 100-mW laser the steady-state transmittance was negligible, and the reaction time was faster. Since the fluence-dependent cut-off model [Eq. (2)] is not applicable to CW OPL, it is important to take this into consideration for experimental design.

## 5 Conclusions

RSA materials' strengths and weaknesses mesh well with the requirements placed on practical laser protection systems since attenuated radiation is not recollected by following optics. This tutorial has demonstrated what the most important photophysical parameters are for RSA materials and their impact on OPL performance. The OPL for different temporal parts of the pulse is influenced differently by the parameters, linear singlet absorption at the start of the pulse while the triplet linear absorption and two-photon singlet absorption influence the important leading edge of the pulse. An overview of relevant measurements has been given with a focus on their potential pitfalls and applicability for assessing OPL performance. The correct interpretation of experimental data is vital to understand the population dynamics of the system. The combination of experimental efforts with simple numerical population models is a powerful tool to reach this understanding.

### *Acknowledgments*

We thank Prof. Emeritus Thor Bernt Melø at NTNU for valuable help in the initial design of the triplet ESA measurement system. There are no conflicts of interest to declare. This work was supported by the Swedish Armed Forces

### *References*

1. C. J. Campbell et al., "The threshold of the retina to damage by laser energy," *Arch. Ophthalmol.* **76**(3), 437–442 (1966).
2. G. L. Wood et al., "Evaluation of passive optical limiters and switches," *Proc. SPIE* **1105**, 154–180 (1989).
3. G. Ritt, S. Dengler, and B. Eberle, "Protection of optical systems against laser radiation," *Proc. SPIE* **7481**, 74810U (2009).
4. G. Ritt and B. Eberle, "Protection concepts for optronical sensors against laser radiation," *Proc. SPIE* **8185**, 81850G (2011).
5. M. J. Miller, A. G. Mott, and B. P. Ketchel, "General optical limiting requirements," *Proc. SPIE* **3472**, 24–30 (1998).
6. D. Dini, M. J. F. Calvete, and M. Hanack, "Nonlinear optical materials for the smart filtering of optical radiation," *Chem. Rev.* **116**(22), 13043–13233 (2016).
7. P. B. Chapple et al., "Single-beam z-scan: measurement techniques and analysis," *J. Nonlinear Opt. Phys. Mater.* **6**(3), 251–293 (1997).
8. J. A. Hermann, "Beam propagation and optical power limiting with nonlinear media," *J. Opt. Soc. Am. B* **1**(5), 729 (1984).
9. L. W. Tutt and T. F. Boggess, "A review of optical limiting mechanisms and devices using organics, fullerenes, semiconductors and other materials," *Prog. Quantum Electron.* **17**(4), 299–338 (1993).
10. Y. B. Band, "Optical properties and applications of reverse saturable absorbers," in *Methods of Laser Spectroscopy*, Y. Prior, A. Ben-Reuven, and M. Rosenbluh, Eds., pp. 117–121, Springer US, Boston, Massachusetts (1986).
11. T. J. McKay, J. A. Bolger, and J. Staromlynska, "Linear and nonlinear optical properties of platinum-ethynyl," *Appl. Phys. B* **108**(13), 5537–5541 (1998).
12. M. G. Vivas et al., "Understanding the two-photon absorption spectrum of PE2 platinum acetylide complex," *J. Phys. Chem. A* **118**(30), 5608–5613 (2014).
13. T. Xia et al., "Optimization of optical limiting devices based on excited-state absorption," *Appl. Opt.* **36**(18), 4110–4122 (1997).
14. T. F. Boggess et al., "Picosecond investigations of optical limiting mechanisms in King's complex," *Opt. Eng.* **32**(5), 1063–1067 (1993).
15. K. McEwan et al., "Synthesis, characterization, and nonlinear optical study of metalloporphyrins," *Adv. Funct. Mater.* **13**(11), 863–867 (2003).
16. W. Blau et al., "Reverse saturable absorption in tetraphenylporphyrins," *Opt. Commun.* **56**(1), 25–29 (1985).
17. Y. Bretonniére and C. Andraud, "Chromophores for optical power limiting," in *Photosensitizers in Medicine, Environment, and Security*, T. Nyokong and V. Ahsen, Eds., pp. 619–654, Springer, Netherlands, Dordrecht (2012).
18. A. Eriksson, *Modeling and Characterization of Nonlinear Materials for Protection of Optical Sensors*, Linköping University, Linköping (2001).
19. E. Glimsdal, *Spectroscopic Characterization of Some Platinum Acetylide Molecules for Optical Power Limiting Applications*, Norwegian University of Science and Technology, Trondheim (2009).
20. S. R. Mishra et al., "The role of non-linear scattering in optical limiting in C60 solutions," *J. Phys. B At. Mol. Opt. Phys.* **27**, L157–L163 (1994).
21. T. Zhang et al., "Enhanced optical limiting performance of a novel molybdenum complex of fullerene," *Opt. Commun.* **150**(1–6), 201–204 (1998).
22. G.-J. Zhou and W.-Y. Wong, "Organometallic acetylides of Pt(II), Au(I) and Hg(II) as new generation optical power limiting materials," *Chem. Soc. Rev.* **40**, 2541–2566 (2011).
23. G. J. Zhou et al., "White metallopolyynes for optical limiting/transparency trade-off optimization," *Angew. Chemie Int. Ed.* **45**(37), 6189–6193 (2006).
24. R. Westlund et al., "Efficient nonlinear absorbing platinum(II) acetylide chrompphores in solid PMMA matrices," *Adv. Funct. Mater.* **18**(13), 1939–1948 (2008).
25. E. E. Silverman et al., "The triplet state in Pt-acetylide oligomers, polymers and copolymers," *Coord. Chem. Rev.* **249**(13–14), 1491–1500 (2005).
26. G. J. Zhou et al., "Optical power limiters based on colorless di-, oligo-, and polymetallaynes: highly transparent materials for eye protection devices," *Adv. Funct. Mater.* **17**(6), 963–975 (2007).
27. J. E. Rogers et al., "Platinum acetylide two-photon chromophores," *Inorg. Chem.* **46**(16), 6483–6494 (2007).
28. J. Staromlynska, T. J. McKay, and P. Wilson, "Broadband optical limiting based on excited state absorption in Pt:ethynyl," *J. Appl. Phys.* **88**(4), 1726–1732 (2000).
29. T. J. Mckay et al., "Cross sections for excited-state absorption in a Pt: ethynyl complex," *J. Opt. Soc. Am. B* **18**(3), 358–362 (2001).
30. D. Chateau et al., "Silica hybrid sol-gel materials with unusually high concentration of ptorganic molecular guests: studies of luminescence and nonlinear absorption of light," *ACS Appl. Mater. Interfaces* **4**(5), 2369–2377 (2012).
31. R. S. Price et al., "Polymer monoliths containing two-photon absorbing phenylenevinylene platinum(II) acetylide chromophores for optical power limiting," *ACS Appl. Mater. Interfaces* **7**(20), 10795–10805 (2015).
32. A. H. Shelton et al., "High efficiency platinum acetylide nonlinear absorption chromophores covalently linked to poly(methyl methacrylate)," *Appl. Mater. Interfaces* **5**, 7867–7874 (2013).
33. H. Lundén et al., "Dispersion and self-orientation of gold nanoparticles in sol-gel hybrid silica–optical transmission properties," *J. Mater. Chem. C* **3**(5), 1026–1034 (2015).

34. D. Chateau et al., "Long distance enhancement of nonlinear optical properties using low concentration of plasmonic nanostructures in dye doped monolithic sol-gel materials," *Adv. Funct. Mater.* **26**, 6005–6014 (2016).
35. H. Lundén et al., "Efficient reverse saturable absorption of sol-gel hybrid plasmonic glasses," *Opt. Mater.* **69**, 134–140 (2017).
36. M. Pokrass et al., "Nonlinear optical and electrical conductivity properties of carbon nanotubes (CNT) doped in sol-gel matrices," *Proc. SPIE* **9168**, 916807 (2014).
37. X. Zheng, M. Feng, and H. Zhan, "Giant optical limiting effect in ormosil gel glasses doped with graphene oxide materials," *J. Mater. Chem. C* **1**(41), 6759 (2013).
38. S. Hirata et al., "Large reverse saturable absorption under weak continuous incoherent light," *Nat. Mater.* **13**(10), 938–946 (2014).
39. M. A. Filatov, S. Baluschev, and K. Landfester, "Protection of densely populated excited triplet state ensembles against deactivation by molecular oxygen," *Chem. Soc. Rev.* **45**(17), 4668–4689 (2016).
40. Y. Bai et al., "Molecular road map to tuning ground state absorption and excited state dynamics of long-wavelength absorbers," *J. Am. Chem. Soc.* **139**(46), 16946–16958 (2017).
41. C. Yao et al., "Platinum(II) acetylide complexes with star- and V-shaped configurations possessing good trade-off between optical transparency and optical power limiting performance," *J. Mater. Chem. C* **5**(45), 11672–11682 (2017).
42. M. G. Vivas et al., "Interpreting strong two-photon absorption of PE3 platinum acetylide complex: double resonance and excited state absorption," *ACS Photonics* **1**(2), 106–113 (2014).
43. A. Eriksson, K. Bertilsson, and M. Lindgren, "Simulation of beam propagation with time-dependent nonlinear processes in optical limiting applications," *Synth. Met.* **127**(1–3), 147–150 (2002).
44. Q. Miao et al., "Dynamical propagation of nanosecond pulses in naphthalocyanines and phthalocyanines," *Chem. Phys.* **480**, 12–16 (2016).
45. Y. Morel et al., "Optical power limiting properties of organic crystals and nanocrystals in an f/5 optical system," *Synth. Met.* **109**, 215–218 (2000).
46. D. B. James and K. J. McEwan, "Bubble and refractive processes in carbon suspensions," *Nonlinear Opt.* **21**, 377–389 (1999).
47. D. Vincent and J. Cruickshank, "Optical limiting with C60 and other fullerenes," *Appl. Opt.* **36**(30), 7794–7798 (1997).
48. R. C. Hollins, "Optical limiters: spatial, temporal, and spectral effects," *Nonlinear Opt.* **21**, 49–61 (1999).
49. M. A. Cagigas, P. J. Valle, and M. P. Cagigal, "Super-Gaussian apodization in ground based telescopes for high contrast coronagraph imaging," *Opt. Express* **21**(10), 12744–12756 (2013).
50. J. Staromlynska et al., "Nonlinear optical materials for switching and limiting," *Proc. SPIE* **2229**, 59–66 (1994).
51. A. Donval et al., "Optical power control filters: from laser dazzling to damage protection," *Proc. SPIE* **8257**, 82570X (2012).
52. F. Meinardi et al., "Highly efficient large-area colourless luminescent solar concentrators using heavy-metal-free colloidal quantum dots," *Nat. Nanotechnol.* **10**(10), 878–885 (2015).
53. M. Sheik-Bahae et al., "Sensitive measurements of optical nonlinearities using a single beam," *IEEE J. Quantum Electron.* **26**(4), 760–769 (1990).
54. *10110-4 Material Imperfections–Inhomogeneity and Striae*, International Organization for Standardization, Genève, Switzerland (1997).
55. F. E. Hernández et al., "Viscosity dependence of optical limiting in carbon black suspensions," *Appl. Opt.* **41**(6), 1103–1107 (2002).
56. D. J. Hagan et al., "Optimization of reverse saturable absorber limiters: material requirements and design considerations," in *Materials Research Society Symp. Proc.*, Vol. 374, pp. 161–172 (1995).
57. M. R. Ferdinandus et al., "Dual-arm Z-scan technique to extract dilute solute nonlinearities from solution measurements," *Opt. Mater. Express* **2**(12), 1776 (2012).
58. D. A. Oulianov et al., "Investigation of benzoporphyrin and azulenic compounds by two-dimensional Z-scan technique," *Proc. SPIE* **3472**, 98–105 (1998).
59. E. W. V. Stryland and M. Sheik-Bahae, "Z-scan measurements of optical nonlinearities," in *Characterization Techniques and Tabulations for Organic Nonlinear Materials(3)*, M. G. Kuzyk and C. W. Dirk, Eds., pp. 655–692, Marcel Dekker, Inc., New York (1998).
60. Y.-L. Huang et al., "Femtosecond Z-scan measurement of GaN," *Appl. Phys. Lett.* **75**(22), 3524–3526 (1999).
61. N. Munera et al., "Broadband near infrared supercontinuum for Z-scan nonlinear spectrometer," in *Frontiers in Optics 2017*, Optical Society of America (2017).
62. R. Wang and J. Wei, "Accurate determination of optical nonlinear absorption coefficients by the combination of reflection and transmission open-aperture z-scan measurements," *Opt. Commun.* **297**, 121–124 (2013).
63. A. S. Marshall, "Nonlinear optical characterization of organic polymers and small molecules and their application towards optical power limiting," Doctoral Dissertation, Georgia Institute of Technology (2014).
64. V. V. Vanyukov et al., "Concentration dependence of the optical limiting and nonlinear light scattering in aqueous suspensions of detonation nanodiamond clusters," *Opt. Mater.* **37**, 218–222 (2014).
65. K. Mansour and E. W. Van Stryland, "Nonlinear optical properties of carbon-black suspensions (ink)," *J. Opt. Soc. Am. B* **9**(7), 1100–1109 (1992).
66. F. Nifiatis et al., "Comparison of the photophysical properties of a planar, PtOEP, and a nonplanar, PtOETPP, porphyrin in solution and doped films," *J. Phys. Chem. A* **115**(47), 13764–13772 (2011).
67. B. Minaev, E. Jansson, and M. Lindgren, "Application of density functional theory for studies of excited states and phosphorescence of platinum(II) acetylides," *J. Chem. Phys.* **125**(9), 94306 (2006).
68. E. Glimsdal et al., "Luminescence, singlet oxygen production, and optical power limiting of some diacetylide platinum(II) diphosphine complexes," *J. Phys. Chem. A* **114**(10), 3431–3442 (2010).
69. P. Lind et al., "Structural, photophysical, and nonlinear absorption properties of trans-di-arylalkynyl platinum(II) complexes with phenyl and thiophenyl groups," *J. Phys. Chem. A* **111**(9), 1598–1609 (2007).
70. M. Lindgren et al., "Electronic states and phosphorescence of dendron functionalized platinum(II) acetylides," *J. Lumin.* **124**(2), 302–310 (2007).
71. G. A. Crosby and J. N. Demas, "Measurement of photoluminescence quantum yields. Review," *J. Phys. Chem.* **75**(8), 991–1024 (1971).
72. W. H. Melhuish, "Quantum efficiencies of fluorescence of organic substances: effect of solvent and concentration of the fluorescent solute," *J. Phys. Chem.* **65**(2), 229–235 (1961).
73. P. G. Seybold, M. Gouterman, and J. Callis, "Calorimetric, photometric and lifetime determinations of fluorescence yields of fluorescein dyes," *Photochem. Photobiol.* **9**(3), 229–242 (1969).
74. G. A. Reynolds and K. H. Drexhage, "New coumarin dyes with rigidized structure for flashlamp-pumped dye lasers," *Opt. Commun.* **13**(3), 222–225 (1975).
75. N. S. Makarov, M. Drobizhev, and A. Rebane, "Two-photon absorption standards in the 550–1600 nm excitation wavelength range," *Opt. Express* **16**(6), 4029–4047 (2008).
76. C. Xu and W. W. Webb, "Measurement of two-photon excitation cross sections of molecular fluorophores with data from 690 to 1050 nm," *J. Opt. Soc. Am. B* **13**(3), 481–491 (1996).
77. E. Glimsdal et al., "Excited states and two-photon absorption of some novel thiophenyl Pt(II)-ethynyl derivatives," *J. Phys. Chem. A* **111**(2), 244–250 (2007).
78. M. A. Albota, C. Xu, and W. W. Webb, "Two-photon fluorescence excitation cross sections of biomolecular probes from 690 to 960 nm," *Appl. Opt.* **37**(31), 7352–7356 (1998).
79. E. Glimsdal et al., "Triplet excited states of some thiophene and triazole substituted platinum (II) acetylide chromophores," *J. Phys. Chem. A* **113**(14), 3311–3320 (2009).
80. G. Ramakrishna et al., "Ultrafast intersystem crossing: excited state dynamics of platinum acetylide complexes," *J. Phys. Chem. C* **113**(3), 1060–1066 (2009).
81. C. Liao et al., "Photoinduced charge separation in platinum acetylide oligomers," *J. Phys. Chem. B* **114**(45), 14763–14771 (2010).
82. R. Liu et al., "Tuning photophysical properties and improving nonlinear absorption of Pt(II) diimine complexes with extended π-conjugation in the acetylide ligands," *J. Phys. Chem. A* **117**(9), 1907–1917 (2013).
83. J. E. Rogers et al., "Photophysical characterization of a series of platinum (II) -containing phenyl-ethynyl oligomers," *J. Phys. Chem. A* **106**, 10108–10115 (2002).
84. H. Lundén, *Sol-Gel Glasses Doped with Pt-Acetylides and Gold Nanoparticles for Enhanced Optical Power Limiting*, Linköping University Electronic Press, Linköping (2017).
85. T. J. Mckay et al., "Nonlinear luminescence spectroscopy in a Pt:ethynyl compound," *J. Appl. Phys.* **85**, 1337–1341 (1999).



**Hampus Lundén** is a doctoral candidate in applied optics at Linköping University (LiU) while working at the Swedish Defence Research Agency (FOI). In 2010, he received his MSc degree in engineering physics from Royal Institute of Technology (KTH) and in 2017 a Tekn. Lic. in Applied Optics from LiU. Current research interests include protection against laser damage and laser-based detection of hazardous materials.

**Eirik Glimsdal** is a principal scientist at the Norwegian Defence Research Establishment (FFI), where he is working with research and development in the field of infrared technology for different applications for the Norwegian Armed Forces. He is a former PhD student at the Department of Physics at the Norwegian University of Science and Technology (NTNU), working on laser-based spectroscopy and photophysical characterization of nonlinear absorbing materials.

**Mikael Lindgren** is a professor in physics at the Norwegian University of Science and Technology (Applied Optics Group/Biophysics Group) since 2003. The current research at NTNU is focused on laser-based spectroscopy, time-resolved optical spectroscopies, and related spectroscopic imaging techniques. Development of spectroscopic

and imaging techniques is applied in biomedical applications and to elucidate biophysical processes. Spectroscopy is used to understand biomolecular and hybrid organic–inorganic nanomaterial systems.

**Cesar Lopes** is a senior research scientist and project manager at the Swedish Defence Research Agency. He received his PhD in inorganic chemistry from Chalmers University of Technology, Gothenburg, Sweden, in 1997. His research interests include optical power limiting materials, phase-change materials, glass materials, and sol–gel technology. Laser-material interactions are studied for application in protection of optical sensors against laser radiation.